The final Published version of the paper is: V. Queral, Design, construction and validation of the UST_1 modular stellarator, *Fusion Engineering and Design* 112 (2016) 410-417.

Link: https://doi.org/10.1016/j.fusengdes.2016.06.039

Design, construction and validation of the UST_1 modular stellarator

V. Queral

Laboratorio Nacional de Fusión, CIEMAT, 28040 Madrid, Spain

Stellarator advancement is hindered, among others, by the requirement of geometric complexity at high accuracy and the still scarce universities and research centres following the stellarator line. In this framework, the objectives of the small UST_1 stellarator development were to: i) explore and test the performance of one possible accurate construction method for stellarators, ii) encourage universities and small fusion research centres to build simple and economical stellarators, iii) educative purpose. Therefore, UST_1 was properly designed to be easily built by a milling machine working on toroidal coordinates, being the winding surface circular poloidally and toroidally. The coil frame is a sole monolithic toroidal thick surface equipped with grooves mechanised by the toroidal milling machine. Only one double pancake is wound in each groove so as to compress the conductor on the laterals of the groove in order to speed up and simplify the winding process. The physics design, the conceptual engineering design and the construction process of UST_1 is presented. The toroidal milling machine is described. The e-beam field line mapping experiments carried out to validate the resulting magnetic configuration are reported. The developed construction method has been proved for the small UST_1 stellarator. Small stellarators are valuable for quick tests of diagnostics, educative purposes, assessment of new confinement concepts, turbulence studies and other applications.

Keywords: stellarator ; fabrication ; toroidal milling ; coil ; e-beam mapping

1. Introduction

Stellarators demand both geometrically complex and highly accurate components, hampering fabrication and increasing cost. Tokamaks require accurate components of simpler shapes. Stellarators might increase the potential as fusion reactors if construction methods, particularly devised for stellarators, were developed. Also, most of the current tokamaks have some drawbacks like the complication of plasma control, current drive complexity and maintenance, high power recirculation and fatigue of materials.

In this framework, the paper summarizes the development and validation of UST_1 (Ultra Small Torus 1), a small modular stellarator. The main objectives of the work were to contribute to the development of new simpler, lower cost and faster construction methods for stellarators and to produce demonstration effect. Demonstration effect is important so as to encourage plasma research groups in universities and small laboratories to build experimental stellarators. If the developed construction method were only feasible for small stellarators, still small stellarators are valuable for the assessment of new confinement concepts, turbulence studies, quick tests of diagnostics and formation.

Simplicity and early integration of the design with the fabrication methods were pursued from the very beginning. Therefore, the design of the stellarator is as important as the methodology used to build it.

The first insight for the UST_1 design came mainly from the CTH coil frames [1], W7-X coils [2] and the modular coils depicted in Ref. [3]. In the end, UST_1 resulted somewhat geometrically similar to a CTH torsatron using modular coils and having the plasma shape similar to LHD torsatron.

UST_1 is a two field period compact modular stellarator with aspect ratio 6, plasma major radius R = 125 mm and 12 resistive modular coils wound in a monolithic plaster frame located around the vacuum vessel. A Java code was developed to partially optimize the definition of the modular coils and perform other calculations. A toroidal milling machine was developed on purpose to mechanize the modular coils. Design magnetic field at axis is B_0 = 90 mT. Plasma heating is produced by a 0.8 kW 2.45 GHz ECRH system.

The physics and engineering conceptual design of the device are presented in Section 2. The engineering details on the vacuum vessel, manufacturing process of the coil frame and the toroidal milling machine are described in

Section 3. The vacuum system, control system, ECRH heating system and power supplies are outlined in Section 4. Further information about the toroidal milling machine and the systems is found in Refs. [4,5]. Finally the e-beam field mapping experiments carried out to validate the performance are shown in Section 5.

The work was funded by the author and developed in his personal laboratory from year 2005 to 2007 and it has to be understood in the framework of low funds and human resources. Therefore, the relevance of the work is based on the conceived methods and the high degree of simplicity achieved, not on the size of the device or the plasma performance. The review of the work and experiences learned are presented now since UST_1 will be dismantled in brief and replaced by UST_2 stellarator, partially based on the UST_1 development.

2. Conceptual design of UST_1

Integration of the physics design, engineering design, and available funds were pursued from the very beginning in an iterative design process. For example, the aspect ratio and size of the stellarator was adapted to commercial off-the-shelf pipe for the vacuum vessel. Also, mean on-axis magnetic field was chosen for the low cost 2.45 GHz magnetrons.

Fig. 1 depicts the conceptual design of UST_1.

Table 1 summarizes the properties of UST_1. The rotational transform is selected in the gap below 1/3 to avoid low order rational surfaces. Only the rather low order 2/7 rational surface remains near the plasma edge, Fig. 2.

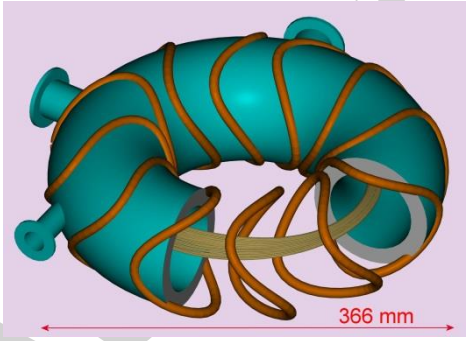

Fig. 1. Sketch of the UST_1 conceptual design.

Element	Specification
Number of periods	2
Plasma volume (litres)	1.1
R, plasma major radius (mm)	125.3
a, ave. plasma minor radius (mm)	21
B_0 Magnetic field on axis (T)	0.089/0.045
ι_0 , rotational transform at axis	0.32
ι_a , rotational transform at edge	0.28

Table 1. Essential properties of UST_1 stellarator

Fig. 2 shows a Poincaré plot of the vacuum magnetic configuration and magnetic islands at two toroidal angles. The black solid line depicts the vacuum vessel. Fig. 3 represents the iota profile. The flatness of the iota profile at r = 21.4 is caused by the island 2/7 (see Fig 2). All the calculations are performed by the Java code named CASTELL (Calculator of stellarators), a series of Java Classes developed from scratch to perform basic calculations based on guiding centre orbit integration.

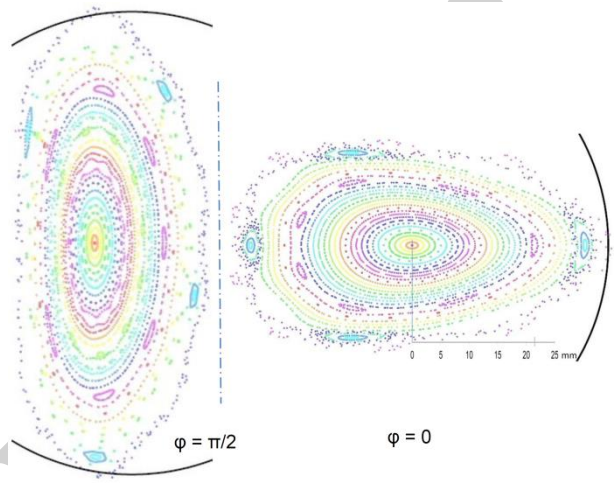

Fig. 2. Poincaré plots for the vacuum magnetic configuration.

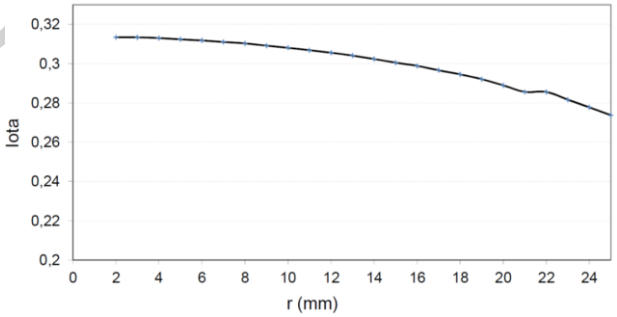

Fig. 3. Iota profile. 'r' is the minor radius on the x+ coordinate axis for each initialised particle.

The coils are defined as grooves mechanized in a thick winding surface so as to avoid the use of winding moulds [6]. Only two turns per layer are wound in the groove. Thus, the conductors are compressed (Fig. 4) on the groove walls to avoid the use of numerous fasteners [7]. The conductor is manufactured from a 6 mm^2 bunch of Cu filaments sleeved in a heatshrink tube 0.3 mm wall thickness, resulting 3.5 mm of external diameter of conductor. The effective copper section in the groove is 50%, a low but acceptable value. Pressure on the wall grooves due to Lorentz force is lower than 10 N/cm^2. Thus, extra conductor fixations or epoxy impregnation is not considered.

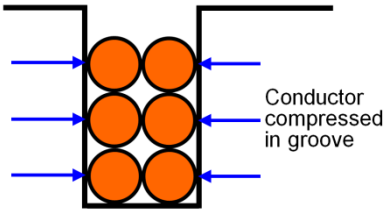

Fig. 4. Concept of two conductors per layer compressed on the walls of the winding groove.

Table 2 summarizes the coil specifications.

Element	Specification
Type of coils	Modular coils
Number of coils	12 (3 shapes)
Turns per coil	6
Shaping Parameters of the coils (p_i)	1.45, 1.3, 1.55, 0.65
Winding pack size (mm)	7 width x 10.5 height
Structure of the winding pack	1 double pancake per coil
Winding surface shape	Circular, poloidally and toroidally
Major / minor radius of winding surface (mm)	119.2 / 57.1

Table 2. Summary of coil specifications.

The expression relating the toroidal and poloidal coordinates of a point of the filamentary coil is:

$$\varphi = \varphi_c - R_0/R \; p \; \lambda \; \sin(2\,\theta)$$

Being:

$$\pi/2\; i < \theta < \pi/2\; (i+1)\; ;\; p = p_i \; ;\; i = 0, \ldots, 3$$

(R, φ, θ) : Toroidal coordinates of each point of the filamentary modular coil. The points are located on a torus of minor radius a = 57.1 mm.

R_0 : Major radius of the toroidal winding surface.

φ_c : Reference toroidal angle position of each coil.

$\varphi_c = 2\pi k/12$, $k = 0, 1, 2$

p_i : Shaping parameters of the coil, e.g. see the shaping parameters shown in Table 2. The shaping parameters of the coil are four parameters defining the amplitude of the sinusoidal deformation of the coil at four quadrants of the poloidal coordinate.

λ : Magnitude of shaping of the coils. $\lambda = 0.15$ for UST_1. Higher λ produce higher rotational transform.

The successive modular coils in each halfperiod turn poloidally by changing the origin of θ coordinate. The origin θ poloidal angle for the successive three modular coils of a halfperiod were selected $\theta_1 = 0$, $\theta_2 = 2\pi/9$, $\theta_3 = 4\pi/9$. The increase approximates to $\pi/5$ corresponding to 5 intervals of 6 coils in one period.

The coils for the other three halfperiods are produced by stellarator symmetry.

A process using the CASTELL code was followed to select the Shaping Parameters shown in Table 2. The winding surface was initially fixed. A four dimensional space of parameters was scanned in three optimization loops. In the first loop a wide interval of parameters was set. Test of 10000 different coil structures lasted about 24 hours of calculations in a PC. Many coil structures were rejected when the calculated rough iota value was found outside the target interval. Accepted coil structures continue calculations of: refined iota at magnetic axis and plasma edge, area of a poloidal section of the plasma volume, standard deviation of the |B| minima values on a magnetic surface, minimum distance between coils, magnetic well and averaged magnetic ripple at axis. At the end of each loop, a spreadsheet was created and the results were ordered according to iota. The coil structures giving iota in the proper iota gap were studied based mainly on the plasma volume and |B| minima standard deviation. New narrower intervals for the four parameters were set heuristically from the best coil structures found and another optimization loop was run. The optimization is modest since the degree of freedom of the coil shapes is constrained on a toroidally and polloidally circular torus.

The final selected modular coils for UST_1 are represented in Fig. 5 in toroidal and poloidal angles. Such coordinates were directly used by the toroidal milling machine for the mechanisation of the grooves.

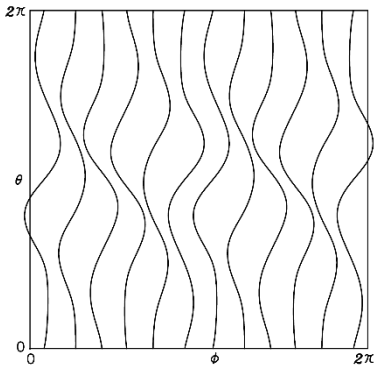

Fig. 5. Contours of UST_1 coils on the winding surface in toroidal and poloidal angles.

3. Engineering design and construction of UST_1

3.1 Vacuum vessel

The vacuum vessel is circular, poloidally and toroidally, with major radius 119.2 mm and minor radius 40 mm. It consists of five commercial 72º copper elbows of 0.8 mm wall thickness externally reinforced with brass rings. Three large perpendicular ports and a small tangential one are available. The components are Sn-Ag soldered and internally thoroughly cleaned. Fig. 6 shows the finished UST_1 vacuum vessel.

Fig. 6. UST_1 vacuum vessel.

3.2 Monolithic coil frame

The frame supporting the grooves for the modular coils is a monolithic frame designed as a sole thick plaster toroidal surface. Common plaster type 'Iberyeso E-35' of experimental hardness Shore D = 50 was utilized. It has enough strength and easy mechanization. The monolithic plaster frame is moulded in two stages in an expanded polystyrene mould (Fig. 7) whose parting plane is the torus equatorial plane. After moulding, the torus is smoothed down by the toroidal milling machine. The result is shown in Fig. 8.

3.3 Coil production and positioning

The positioning of the coils would be unnecessary and the positioning accuracy would be high if the coils were mechanized on the frame by a milling machine. The coil adjustment and metrology worktime would also be avoided.

Fig. 7. Expanded polystyrene mould and vacuum vessel covered by a separation layer.

Fig. 8. Finished smoothed and completely circular monolithic frame without grooves.

In UST_1 twelve grooves 7 mm wide and 12 mm deep (Fig. 9) are mechanized in the plaster frame by the special milling machine working on toroidal coordinates. The groove width is identical to the diameter of the milling cutter so as to produce one groove with only one poloidal turn of the milling head. Thus, the mechanization of each groove was fast and simple. It lasted around 2 hours.

3.4 Coil winding

Following the concept of two conductors per layer compressed on the walls, the conductor (red conductor in Fig. 10) is introduced in the groove together with an auxiliary conductor (black in Fig. 10) used to temporarily fix the first turn of the pair of turns per layer.
The second turn is introduced in the groove (Fig. 10-right) and compressed on the walls of the groove while the auxiliary conductor is unwound. As conceived, the turns do not unwind during the winding process and fasteners were unnecessary.

Each winding pack is formed by 3 layers of 2 turns per layer, resulting 6 turns per modular coil. The final 12 modular coils are shown in Fig. 11.

Fig. 9. Monolithic frame and grooves for the coils.

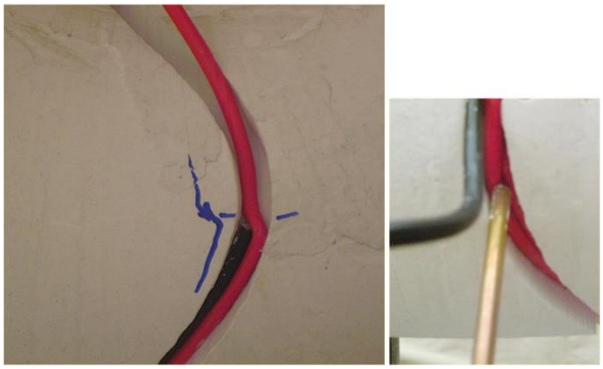

Fig. 10. Starting the first turn of one modular coil (left). Compression on the walls of the groove (right).

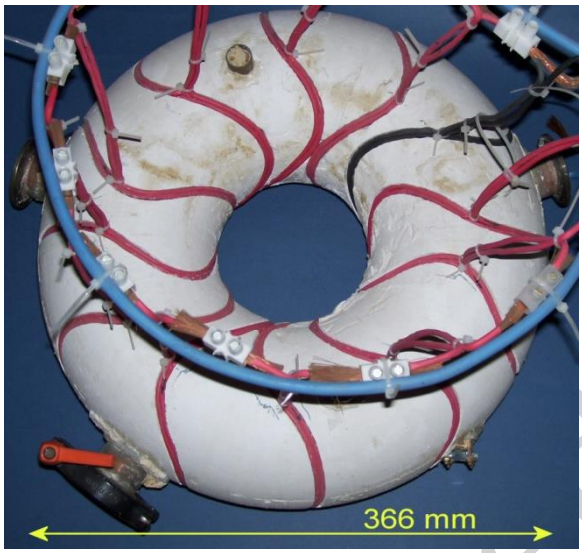

Fig. 11. Plan view of the 12 manufactured modular coils.

3.5 Toroidal milling machine

The concept and implementation of the toroidal milling machine are briefly summarized next. Further information can be found in Ref. [4].

The milling machine is composed of two main elements, Fig. 12: A circular guide and a turning horizontal base. The circular guide allows the circular poloidal movement of the milling head and the turning base gives the toroidal rotation to the stellarator. The toroidal surface remains attached to the turning base during the full mechanisation of all the grooves. This method avoids repositioning of the toroidal surface in order to mechanise inaccessible areas of the winding surface as it would happen with a common milling machine. It increases accuracy and simplifies the milling process. The circular guide is located in a vertical plane and supports a circularly movable circular sector which supports the milling head.

The use of this toroidal milling machine makes unnecessary the positioning and adjustment of the modular coils since the positioning of the grooves is accurate and produced during the mechanisation of the whole monolithic coil frame.

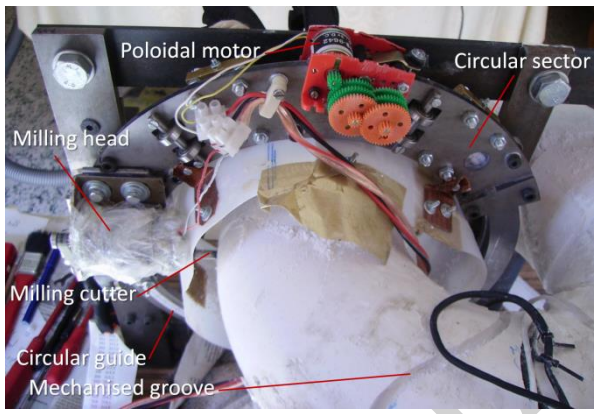

Fig. 12. Detail of the toroidal milling machine.

4. The UST_1 facility

The different systems of the UST_1 facility are outlined next. In spite of the simplicity, the facility is able to evacuate, feed, control, and diagnose the stellarator.

4.1 Vacuum system

The UST_1 vacuum system is composed essentially by a roughing mechanical oil pump Pfeiffer DUO 004A (4 m^3/h), a diffusion pump Leybold (~150 L/s). Vacuum gauges: 'Edwards' active inverted magnetron gauge (1Pa - 10^{-6} Pa), 'Lesker' thermocouple gauge 100 Pa – 0.1Pa, and Bourdon manometer. One 'AMETEK Dycor Quadlink' quadrupole mass spectrometer (RGA) and the necessary fittings and valves. Vacuum level typically reached 5 x 10^{-3} Pa after 30 minutes pumping without baking.

4.2 Power supplies

Seven lead batteries 12 V, 45A-h, are installed in series supplying 400 A to the stellarator. The power generated by the batteries is 35 kW. 19 kW are supplied to the coils and 16 kW are lost in the internal resistance of batteries, connections, main switch and leads. A notable impedance matching for maximum supplied power is achieved. There is no current regulator in the system. As a consequence, the current drops (Fig. 19) ~12% during the pulse due to copper temperature increase and fatigue of the batteries.

4.3 Heating system

Only ECRH heating at 2.45 GHz is installed. The heating system is based on a magnetron from a commercial microwave oven. The waves are transmitted by a coaxial cable and emitted into the vacuum vessel by a ¼ λ stub antenna. The small size of the stellarator hinders the wave injection by a waveguide.

The heating system is composed of the magnetron, a waveguide to coaxial adapter located inside the microwave oven, coaxial cable RG214, a dual directional coupler, two biased Schottky diode detectors to measure the forward and reflected power, a double stub microwave tuner for impedance tuning, HN Type feedthrough, the ¼ lambda stub, several N Type coaxial connectors and two microwave leak detectors.

4.4 Control system

Two PCs are installed, one for the high speed digital camera and one for the slow control of the pulse. A C-language code controlling two A/D cards is able to start/end the power supplies, the ECRH heating, control the e-gun, and carry out data acquisition of the coil current, ECRH power emitted/reflected and vacuum level. The vacuum system is controlled manually.

4.5 Diagnostics

The available diagnostics are:
- Digital camera of 400Mb/s Firewire transmission, 30 fps, 640 x 480 pixels, non-compressed image.
- E-beam field mapping system.
- Langmuir probe.
- Residual gas analyser.

Not all the diagnostics can be installed and used simultaneously due to the reduced number of ports.

Fig. 13 displays a picture of the facility during e-beam field mapping experiments.

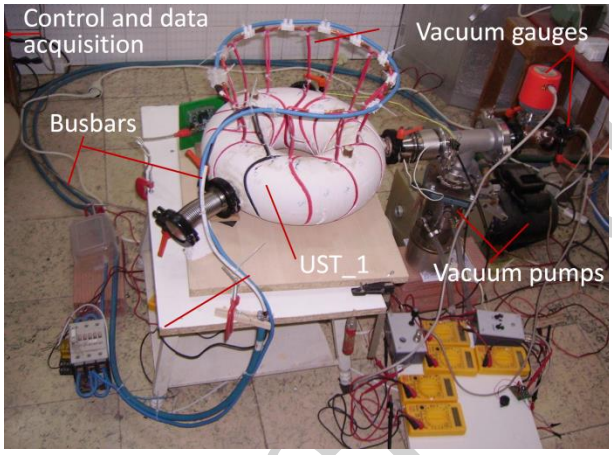

Fig. 13. UST_1 and vacuum system at the facility.

5. E-beam field mapping experiments

E-beam field line mapping experiments were performed to validate the accuracy of the resulting magnetic configuration.

5.1 Set-up of the e-beam field line mapping

The traditional fluorescent movable rod method [8] was implemented. A sketch of the e-beam field mapping experimental setup is shown in Fig. 14.

A very simple mechanism is utilized for the fluorescent rod movement. The rod is a copper wire 1.5 mm diameter and 120 mm long (Fig.15). It is covered with fluorescent doped ZnO powder type P-24-GE, deposited on the wire by a methanol-powder solution. The wire lays equilibrated on a thin tip. A magnetic short pulse supplied from the exterior of the vacuum vessel starts a free oscillation of the rod lasting few seconds. The length of the wire gives a wire oscillation frequency of 2 Hz, appropriate for a pulse length of ~2.5 s and 30 fps frame rate of a digital camera. The camera is a Unibrain Fire-i, 400Mb/s Firewire transmission speed installed at the port P4. Optical deformation of the images is low due to nearly perpendicular focussing on the rod.

The achieved simplicity of the mechanism is one of the results of the work.

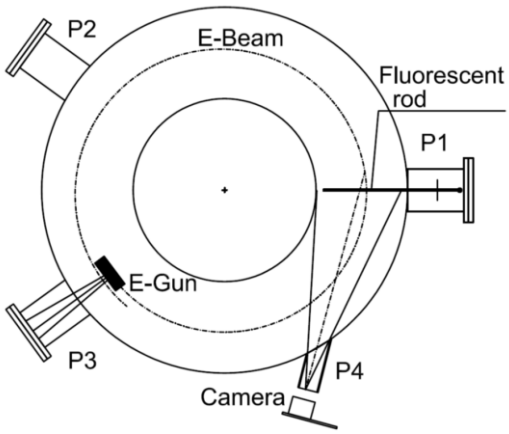

Fig. 14. Field line mapping experimental setup.

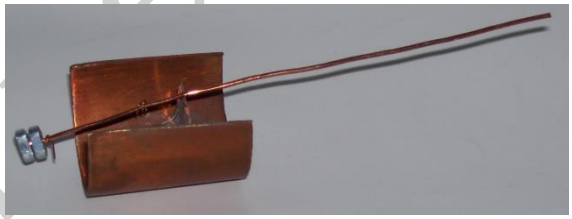

Fig. 15. Oscillating fluorescent rod.

Fig. 16 shows the two models of e-gun built and used during the experiments. Each e-gun is built from a cut 10 W, 12 V commercial halogen light bulb introduced in an internally blackened metallic cover. The extraction hole is 1.25 mm diameter and the distance from the filament to the extraction hole ~0.75 mm.

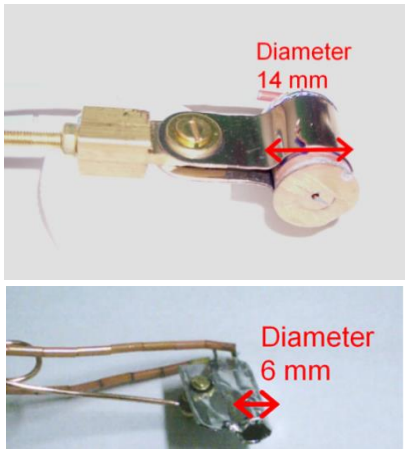

Fig. 16. 14 mm diameter e-gun model 'E-Gun-2' (top) and 6 mm 'E-Gun-3' (bottom).

Several difficulties appeared during the e-beam experimental sessions, among them:

- The e-beam collided with the rear part of the e-gun after the third turn of the beam since the rotational transform is approximately of 1/3. Due to the small size of UST_1 this issue was challenging. Accurate strategic positioning of the tiny E-Gun-3 was required to solve the issue.
- The E-Gun-3 was fragile and gave lower beam current and higher background light than E-Gun-2.
- The low sensitivity of the camera hardly recorded the fluorescent points. Relatively high electron energy (~100 eV) was set for higher brightness but large drifts appear due to the small size of UST_ 1 (small curvature radius) and low B_0.

5.2 Comparison between experimental results and calculations

Pulses #198 and #202 showed more than three fluorescent points of enough luminosity to be recorded by the camera. Fig. 17 shows the superposition of 12 frames obtained from the pulse #202 (24-08-2006). The experimental conditions during pulse #202 were: B_0 = 34 mT, acceleration voltage 95 V, vacuum level 3 x 10^{-3} Pa. Fig. 18 superposes the calculated and experimental beam-rod intersections. Point 1 (Fig. 18) faded due to the frame superposition process but it is visible in the original video recording. Points 4 and 7 are outside the oscillating rod area and are not recorded. The reason for the invisibility of point 8 is unknown. The small size of the stellarator and the poor quality of the e-guns hamper higher precision images.

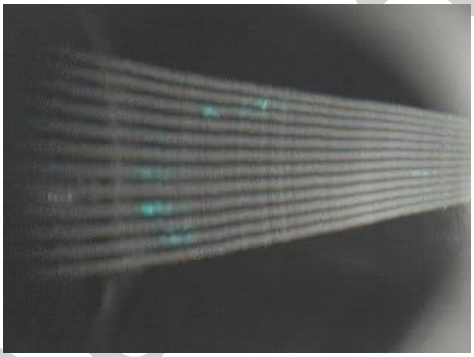

Fig. 17. E-beam mapping result from the pulse #202.

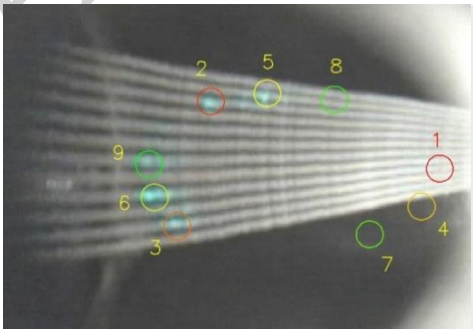

Fig. 18. Comparison of experimental field mapping images (cyan points) and calculated points (circles).

A notable degree of accuracy was achieved in the design and construction of the stellarator since the experimental magnetic surfaces notably agree with the calculated surfaces. Nevertheless, measurement errors of the system are ~±1 mm. Therefore, slight magnetic errors, significant for plasma confinement, may still exist. Thus, the validation of the quality of the construction is only partial.

6. Plasma pulses

After e-beam field mapping, the ECRH system was installed and pulses from #211 to #254 generated plasmas. A chronogram of the pulse #248 is shown in Fig. 19.

The coil current and B_0 decrease with time due to the lack of current regulation. An increase of neutral pressure in the vacuum vessel at the starting of the pulse is observed. Desorption from the walls is the most likely reason. Plasmas did not achieve any satisfactory degree of purity.

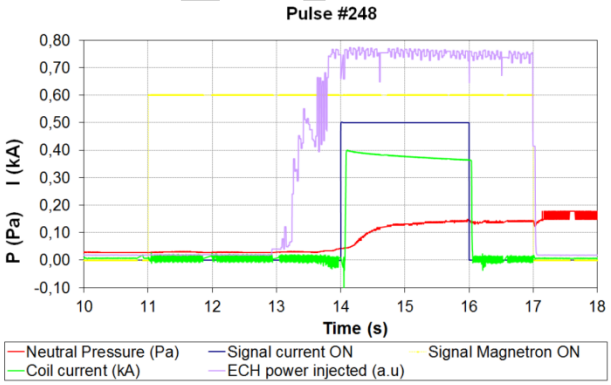

Fig. 19. Chronogram of pulse #248.

7. Cost and worktime breakdown

The total cost of the materials used in the facility was about 4000 € (€ year 2006). Most of the elements were second hand ones. The vacuum system was the most expensive system, accounting for 50% of the budget.

Worktime is divided between R&D time and construction/installation time. The two types of worktime are somewhat mixed.

A database accounting the different daily activities was filled during the project development. The author performed all the activities cited next. In July 2005 started the conception of the stellarator. In August 2006 satisfactory magnetic surfaces had already been obtained. The total worktime during such period was 2606 hours.

Table 3 shows the time breakdown of the different concepts accounted.

Activity	Dedicated time (hours)
1. Develop CASTELL code, optimize coils.	440
2. Vacuum: Formation, orders, assembly, leak test.	378
3. Toroidal milling machine: Conception, design, tests and construction.	264
4. General formation, calculations, devise.	196
5. Search components, orders.	158
6. E-guns: Formation, construction, installation.	105
7. Vacuum vessel: Devise, design, solder parts.	102
8. Coil monolithic frame: Design, test, production.	46
9. Conductor manufacture. Modular coil design and test. Integration.	54
10. Mechanize the grooves in the plaster frame.	35
11. Other activities.	828
TOTAL	2606

Table 3. Worktime breakdown of the activities.

The cost of the raw materials for the UST_1 stellarator torus alone is negligible compared with the construction time cost. It is common in most of the one-of-a-kind complex devices.

The time used for modular coils definition and fabrication (including design and construction of the toroidal milling machine), and the development of the vacuum system are the bulk of the worktime.

8. Experiences learned

The experiences learned are listed next. They are focused on the construction of a new small stellarator.

- Winding one turn per layer compressed in the groove is simpler and faster than winding two turns per layer due to the need of an auxiliary conductor (Fig. 9). Utilization of one turn per winding pack layer should be pursued if the required effective copper section is modest.
- The manufacture of the special sleeved conductor was time costly. Thin wall commercial copper conductors are available for a few ranges of diameters. For example, the commercial TXL 10 Gauge copper wire almost achieves the effective Cu section of the special conductor used in UST_1.
- An improved, but still low cost vacuum vessel construction method, should be devised and tested. It is challenging since the manufacture of convoluted stellarator vacuum vessels is usually complex and expensive [9,10,11]. Excessive desorption during pulses and excessive outgassing is the main issue of the UST_1 vacuum vessel.
- The toroidal milling machine is unsuited for very convoluted winding surfaces. Additive manufacturing methods might be superior to the subtractive construction method presented here.
- The toroidal milling machine is expensive if at least several similar stellarators are not fabricated.
- UST_1 is incapable for valuable plasma experiments. A stellarator scaled at least three-fold UST_1 might be able for worthy plasma experiments. For example the small Tohoku University Heliac [12] and TJI-U [13] produce useful experimental results [14].

9. Summary of results

- A simple and low cost stellarator has been built and validated.
- Inspiration and encouragement has been generated in other researchers and countries. For example, the SCR-1 stellarator has been built in Costa Rica [15] based on the UST_1 physics and engineering design.
- UST_1 has contributed to the formation of plasma and fusion engineering students.
- A construction method for stellarator coils based on a toroidal milling machine has been developed.
- A particularly simple and economical e-beam field mapping system has been devised and utilized.

10. Conclusions

The design, construction and operation of a low-cost stellarator have been carried out. The know-how generated might be valuable for universities or low budget laboratories.

A special milling machine working on toroidal coordinates has been developed, utilized and validated by the construction of a stellarator.

The combination of a single monolithic frame with grooves and compression of two conductor turns per layer in the groove resulted in simple positioning of the coils and fast winding.

A more equilibrated balance between the materials cost and the worktime cost should be accomplished for a future stellarator.

Further R&D on integration of engineering and physics, and on faster and lower cost construction methods would be worthy, particularly for one-of-a-kind devices like stellarators.

Acknowledgement

The author would like to thank all the companies, friends, and researchers who altruistically contributed during 2005/06 to the UST_1 development, particularly the Berstron® companies (free supply of mechanical and electronic components), Cristobal Belles (IT help), Dr. Jose M. Reynolds (ECRH heating), Dr. G. J. Hartwell (CTH data), and current or former CIEMAT staff, Drs.: Daniel Lopez-Bruna, Victor Tribaldos, Bernardo Zurro, Xavier Sarasola (e-gun construction), Jose A. Ferreira (vacuum), and Jesus A. Romero.

References

[1] G. J. Hartwell, S. F. Knowlton,C. Watts, J. D. Hanson and T. Brown, Design and construction progress of the Compact Toroidal Hybrid, 13th International Stellarator Workshop, Canberra, Australia, 25 February - 1 March 2002, Paper n. PIIB.7, 2002.

[2] C. Beidler, G. Grieger, F. Herrnegger, E. Harmeyer, J. Kisslinger, et al., Physics and engineering design for W7-X, Fusion Technology 17 (1990) 148–167.

[3] T. J. Dolan. Fusion Research, Pergamon Press, p. 398, 1980.

[4] V. Queral, Coil fabrication of the UST 1 modular stellarator and potential enhancements, Fusion Engineering and Design 88 (2013) 683-686.

[5] V. Queral, web site www.fusionvic.org, accessed on October 2015.

[6] K. Risse, Th. Rummel, L. Wegener, R. Holzthüm, N. Jaksic, F. Kerl and J. Sapper, Fabrication of the superconducting coils for Wendelstein 7-X, Fusion Engineering and Design 66-68 (2003) 965-969.

[7] J. H. Chrzanowski, P. J. Fogarty, P. J. Heitzenroeder, T. Meighan, B. Nelson, S. Raftopoulos and D. Williamson, Manufacturing development of the NCSX modular coil windings, Conference proceedings of the Twenty-First IEEE/NPS SOFE 2005, Knoxville, Tennessee, USA, 26-29 September, 2005.

[8] X. Sarasola, T. S. Pedersen, J. P. Kremer, R. G. Lefrancois, Q. Marksteiner and N. Ahmad, Field line mapping results in the CNT stellarator, 32nd EPS Conference on Plasma Physics, Tarragona, Spain, 27 June - 1 July 2005, ECA Vol.29C, P-1.058, 2005.

[9] M.E. Viola, T. Brown, P. Heitzenroeder, W. Reiersen, P. Goranson, et al., NCSX vacuum vessel fabrication, Proceedings of 21st IEEE/NPS Symposium on Fusion Engineering (SOFE 05), Knox-ville, Tennessee (USA), September 2005.

[10] J. Reich, W. Gardebrecht, B. Hein, B. Missal, J. Tretter, M. Wanner, F. Leher and S. Langone, Manufacture of the vacuum vessels and the ports of Wendelstein 7-X, Fusion Engineering and Design 75-79 (2005) 565-569.

[11] N. Inoue, A. Komori, H. Hayashi, H. Yonezu, M. Iima, et al., Design and construction of the LHD plasma vacuum vessel, Fusion Eng. Des. 41 (1998) 331–336.

[12] H. Takahashi, S. Kitajima, M. Yokoyama, Y. Tanaka, H. Utoh, H. Hashizume, M. Sasao and M. Takayama, Configuration Effect on LH Transition in Tohoku University Heliac, J. Plasma Fusion Res. Series 6 (2004) 266-370.

[13] E. Ascasibar, L. Almoguera, J. Alonso, J. Botija, J. Moreno, A.P. Navarro, et al., Engineering design and construction of a low aspect ratio Torsatron: the TJ-Iupgrade, fusion technology, in: Proceedings of the 16th Symposium on FusionTechnology, 3–7 September 1990, 1990, pp. 577–581.

[14] A. Köhn, G. Birkenmeier, E. Holzhauer, M. Ramisch and U. Stroth, Generation and heating of toroidally confined overdense plasmas with 2.45 GHz microwaves, Plasma Phys. Control Fusion 52 (2010) 035003.

[15] V.I. Vargas, J. Mora, J. Asenjo, E. Zamora, C. Otárola, et al., Engineering Issues to the Stellarator of Costa Rica 1, Proceedings of the 25th Symposium on Fusion Engineering, San Francisco, CA (USA), 10-14 June 2013.